Journal of Low Temperature Physics (2024) 214:331–343
https://doi.org/10.1007/s10909-023-03027-4

Non-Markovian Stochastic Gross–Pitaevskii Equation for the Exciton–Polariton Bose–Einstein Condensate

Alexey D. Alliluev[1] · Denis V. Makarov[1] · Norayr A. Asriyan[2,5] · Andrei A. Elistratov[2] · Yurii E. Lozovik[3,4]

Received: 15 August 2023 / Accepted: 9 December 2023 / Published online: 9 January 2024

Abstract
In this paper, a non-Markovian version of the Gross–Pitaevskii equation is proposed to describe the condensate formation in an exciton–polariton system subject to incoherent pumping. By introducing spatially delta-correlated noise terms, we observe a transition from a spatially ordered phase to a disordered one with simultaneous density reduction as the temperature increases. Above the transition temperature, the uniform condensate breaks up into multiple irregularly located separate dense spots. Using the Gabor transform, we demonstrate condensate decoherence with increasing temperature, which is accompanied by the transition from narrow-band to broad-band spectral density.

Keywords Non-Markovian dynamics · Exciton–polaritons · Bose–Einstein condensation · Optical coherence

1 Introduction

Open quantum systems attract much interest in recent years, which is largely due to the rapid development of quantum computing technologies. A common approach for studying such systems is the Markov approximation based on the Lindblad equation for the density matrix or the stochastic Schrödinger equation [1, 2].

✉ Denis V. Makarov
makarov@poi.dvo.ru

1 V. I. Il'ichev Pacific Oceanological Institute, Far East Branch of the Russian Academy of Sciences, Vladivistok, Russia 690041

2 N.L. Dukhov Research Institute of Automatics (VNIIA), Moscow, Russia 127030

3 Institute for Spectroscopy RAS, Troitsk, Russia 108840

4 MIEM, National Research University Higher School of Economics, Moscow, Russia 101000

5 Institute of Microelectronics Technology RAS, Chernogolovka, Russia 142432

When dealing with a condensate of quasiparticles, we can consider it as an open quantum system coupled with a reservoir of non-condensed particles. For a theoretical description, the stochastic Gross–Pitaevskii equation can be used [3, 4]. However, in up-to-date experiments, the reservoir may have a relatively low temperature as well as a narrow energy spectrum. This makes Markovian approximation invalid for such systems. Non-Markovian evolution infers the existence of memory effects in the system. The corresponding evolution equation is an integro-differential one with time non-local terms [5]. For instance, Nakajima–Zwanzig [6, 7] equation or non-Markovian version of the Lindblad equation [8, 9] is used for the density matrix. Though the non-Markovian Schrödinger equation for non-interacting particles was first introduced in [10], generalizing it for systems with interparticle interaction is still a challenge. Significant progress has been made in [11], where, using the Keldysh diagram technique, a system of non-Markovian equations for an exciton–polariton Bose–Einstein condensate in a Fabry–Perot optical microresonator has been derived.

An exciton–polariton is a bound state of an exciton and a photon, with its lifetime being significantly affected by the quality factor of the optical microresonator. Condensation arises as a result of polariton thermalization stimulated by laser pumping. Exciton polaritons are attractive for technological applications largely because of the prospects for their use in quantum computing applications [12], as well as in the context of the polariton laser [13]. In addition, polariton condensate is an excellent playground for observing macroscopic quantum phenomena [14, 15] as well as studying phase transitions. Namely, formation of spatial patterns [16, 17] and decoherence mechanisms [18] are subjects of increasing interest.

In [11], it was assumed that the condensate corresponds to a macroscopically populated state with zero momentum. Therefore, the resulting system of equations may be treated as a discrete non-Markovian Gross–Pitaevskii equation. Unfortunately, a rigorous derivation of a similar Gross–Pitaevskii equation with spatial dynamics taken into account remains challenging. However, as a reasonable approximation, we may extrapolate the evolution equation from [11] on a small neighbourhood of zero-momentum state. This approach corresponds to considering a smoothly varying spatial profile of the macroscopic wave function of the condensate. Under this assumption, one can derive a non-Markovian version of the Gross–Pitaevskii equation for the exciton–polariton condensate.

The paper is organized as follows. In the next section, we introduce the non-Markovian stochastic Gross–Pitaevskii equation. The process of condensate formation is studied in Sect. 3 by means of numerical simulation, which is followed by a statistical analysis in Sect. 4. In the last section, we summarize and discuss the obtained results.

2 Non-Markovian Stochastic Gross–Pitaevskii Equation

When dealing with exciton–polariton condensation, one may usually neglect the population of the upper spectral branch (upper polariton states) [19]. It leads to the following form of the Gross–Pitaevskii equation:

$$i\hbar\frac{\partial\psi(\mathbf{r},t)}{\partial t}=\hat{H}_0\psi(\mathbf{r},t)+P_{\mathrm{coh}}(\mathbf{r},t)+\hat{D}_{\mathrm{cav}}\psi(\mathbf{r},t)+\hat{D}_{\mathrm{ex}}\psi(\mathbf{r},t), \tag{1}$$

where $\hat{H}_0$ is a unitary operator including kinetic and potential energies, and energy corrections due to interparticle interactions,

$$\hat{H}_0=-\frac{\hbar^2}{2m^*}\nabla^2+V(\mathbf{r})+\alpha_{\mathrm{c}}|\psi(\mathbf{r},t)|^2+\alpha_{\mathrm{r}}\rho_{\mathrm{r}}(\mathbf{r},t). \tag{2}$$

Here m^* denotes for the effective polariton mass, which is approximately 10^{-5} –10^{-4} m_{e}, $V(\mathbf{r})$ is the external potential, α_{c} is the interaction constant for condensate polaritons, α_{r} describes condensate–reservoir interaction and $\rho_{\mathrm{r}}(\mathbf{r},t)$ is the exciton reservoir density. The function $P_{\mathrm{coh}}(\mathbf{r},t)$ in (1) describes coherent laser pumping of microresonator photons.

Non-Hermitian operators $\hat{D}_{\mathrm{cav}}$ and $\hat{D}_{\mathrm{ex}}$ correspond to interactions with the photon and exciton reservoirs, respectively. Hereafter, we assume that the interaction with the photon reservoir is Markovian. This assumption leads to

$$\hat{D}_{\mathrm{cav}}\psi=-i\gamma_{\mathrm{cav}}\psi+\eta_{\mathrm{cav}}(\mathbf{r},t). \tag{3}$$

Using the truncated Wigner approximation, one can derive the following expression for the auto-correlation function:

$$\langle\eta^*_{\mathrm{cav}}(\mathbf{r},t)\eta_{\mathrm{cav}}(\mathbf{r}',t')\rangle=\frac{\gamma_{\mathrm{cav}}}{\Delta x\Delta y}\delta(\mathbf{r}-\mathbf{r}')\delta(t-t'), \tag{4}$$

with Δx and Δy being the grid cell sizes.

The non-Markovian behaviour of the system is mainly associated with the interaction with the exciton reservoir. Considering only the low-momentum states as a condensate, we can use the following approximation:

$$\hat{D}_{\mathrm{ex}}\psi(\mathbf{r})\simeq\hbar\int_0^t \mathrm{d}t'\Sigma^{\mathrm{R}}(t,t')\psi(\mathbf{r},t')+\eta_{\mathrm{ex}}(\mathbf{r},t), \tag{5}$$

i.e. treat the retarded self-energy term $\Sigma^{\mathrm{R}}(t,t')$ as a spatially homogeneous one. We use expressions derived in [11]

$$\Sigma^{\mathrm{R}}(t,t')=i\frac{\rho_{\mathrm{r}}^2\alpha_{\mathrm{c}}^2}{\hbar^2}\frac{e^{-\gamma_{\mathrm{ex}}(t-t')}}{1+\left[\frac{k_{\mathrm{B}}T}{\hbar}(t-t')\right]^2}\theta(t-t'), \tag{6}$$

with $\theta(t)$ being the Heaviside function, γ_{ex} is the condensate exciton decay rate. The corresponding expression for the Keldysh component of the self-energy term is as follows:

$$\Sigma^{\mathrm{K}}(t,t') = -i\frac{\rho_{\mathrm{r}}^2\alpha_{\mathrm{c}}^2}{\hbar^2}\frac{e^{-\gamma_{\mathrm{ex}}|t-t'|}}{1+\left[\frac{k_{\mathrm{B}}T}{\hbar}(t-t')\right]^2}. \tag{7}$$

This expression defines the temporal auto-correlation function of exciton fluctuations:

$$\langle \eta^*(\mathbf{r},t)\eta(\mathbf{r}',t')\rangle = i\hbar^2\frac{\delta(\mathbf{r},\mathbf{r}')}{\Delta x\Delta y}\Sigma^{\mathrm{K}}(t,t'). \tag{8}$$

When modelling the spatial structure of exciton fluctuations, we utilize above a simple approximation, considering them as delta-correlated. Condensate formation with spatially correlated noise was studied in [20]. Thus, equation (1) takes the form

$$\begin{aligned} i\hbar\frac{\partial\psi(\mathbf{r},t)}{\partial t} &= \hat{H}_0\psi(\mathbf{r},t) - \frac{i\hbar\gamma_{\mathrm{cav}}}{2}\psi(\mathbf{r},t) + P_{\mathrm{coh}}(\mathbf{r},t) \\ &+ \eta_{\mathrm{cav}}(\mathbf{r},t) + \eta_{\mathrm{ex}}(\mathbf{r},t) + \hbar\int_0^t \mathrm{d}t'\Sigma^{\mathrm{R}}(t,t')\psi(\mathbf{r},t') \end{aligned} \tag{9}$$

In our model, exciton reservoir density evolves as described by the equation

$$\begin{aligned} \frac{\partial\rho(\mathbf{r},t)}{\partial t} &= \frac{1}{\hbar}P_{\mathrm{incoh}}(\mathbf{r},t) - \gamma_{\mathrm{exR}}\rho(\mathbf{r},t) - \frac{2}{\hbar}\mathrm{Im}\left[\psi^*(\mathbf{r},t)\eta(\mathbf{r},t)\right] - \\ &- 2\mathrm{Im}\left[\psi^*(\mathbf{r},t')\int \mathrm{d}t'\Sigma^{\mathrm{R}}(t,t')\psi(\mathbf{r},t')\right], \end{aligned} \tag{10}$$

where the term $P_{\mathrm{incoh}}(\mathbf{r},t)$ describes the incoherent pumping of the reservoir, and γ_{exR} is the reservoir exciton decay rate. The third term on the right-hand side describes polariton exchange between the condensate and the reservoir due to fluctuations.

In [21], we have demonstrated that at low temperatures, an exponential approximation can be used both for (6) and (7):

$$\Sigma^{\mathrm{R}}(t,t') \simeq i\frac{\rho_{\mathrm{r}}^2\alpha_{\mathrm{c}}^2}{\hbar^2}e^{-\gamma_{\mathrm{eff}}(t-t')}\theta(t-t'), \tag{11}$$

$$\Sigma^{\mathrm{K}}(t,t') \simeq -i\frac{\rho_{\mathrm{r}}^2\alpha_{\mathrm{c}}^2}{\hbar^2}e^{-\gamma_{\mathrm{eff}}|t-t'|}. \tag{12}$$

Moreover, for low temperatures, γ_{eff} is linearly dependent on temperature [20]. In this case, the auto-correlation function (8) corresponds to the complex-valued stochastic Ornstein–Uhlenbeck process, when $\tilde{\eta}(\mathbf{r},t)$ is the solution of the following Langevin equation:

$$\frac{d\tilde{\eta}(\mathbf{r},t)}{dt} = -\gamma_{\mathrm{eff}}\tilde{\eta}(\mathbf{r},t) + \sqrt{2\gamma_{\mathrm{eff}}}\xi(\mathbf{r},t). \tag{13}$$

Here $\xi(\mathbf{r},t)$ is a complex white noise with unit variance,

$$\langle \xi^*(\mathbf{r},t)\xi(\mathbf{r}',t')\rangle = \delta(t-t')\delta(\mathbf{r}-\mathbf{r}'). \tag{14}$$

The exponential form of the memory kernel in (9) allows introducing an auxiliary wave function ϕ to transform the equation into an equivalent Markov equation:

$$\phi(\mathbf{r},t) = \psi_0(\mathbf{r})e^{-\gamma_{\text{eff}}t} + \int_0^t \mathrm{d}t' e^{-\gamma_{\text{eff}}(t-t')}\psi(\mathbf{r},t'), \tag{15}$$

where $\psi_0(\mathbf{r}) = \psi(\mathbf{r}, t=0)$. This technique is known as Markov embedding [5, 22]. The equations (9) and (10) are now expressed as follows:

$$\begin{aligned} i\hbar\frac{\partial\psi(\mathbf{r},t)}{\partial t} &= \hat{H}_0\psi(\mathbf{r},t) - \frac{i\hbar\gamma_{\text{cav}}}{2}\psi(\mathbf{r},t) + P_{\text{coh}}(\mathbf{r},t) + \eta(\mathbf{r},t) + \\ &+ i\frac{\alpha_{\text{c}}^2\rho_{\text{r}}^2(\mathbf{r},t)}{\hbar\gamma_{\text{eff}}}\left[\phi(\mathbf{r},t) - \psi_0(\mathbf{r})e^{-\gamma_{\text{eff}}t}\right], \end{aligned} \tag{16}$$

$$\begin{aligned} \frac{\partial\rho_{\text{r}}(\mathbf{r},t)}{\partial t} &= \frac{1}{\hbar}P_{\text{incoh}}(\mathbf{r}) - \gamma_{\text{exR}}\rho_{\text{r}}(\mathbf{r},t) - \frac{2}{\hbar}\mathrm{Im}\{\psi^*(\mathbf{r},t)\eta(\mathbf{r},t)\} - \\ &- 2\frac{\alpha_{\text{c}}^2\rho_{\text{r}}^2(\mathbf{r},t)}{\hbar^2}\mathrm{Re}\left\{\psi^*(\mathbf{r},t)\left[\phi(\mathbf{r},t) - \psi_0(\mathbf{r})e^{-\gamma_{\text{eff}}t}\right]\right\}. \end{aligned} \tag{17}$$

These equations have to be supplemented with the evolution equation for the auxiliary wave function ϕ:

$$\frac{\partial\phi(\mathbf{r},t)}{\partial t} = \gamma_{\text{eff}}[\psi(\mathbf{r},t) - \phi(\mathbf{r},t)]. \tag{18}$$

3 Numerical Simulation

In the present paper, the system of equations (17–18) is used to study condensate formation in a polariton gas exposed to incoherent pumping, i.e. in the absence of direct coherent photon pumping into the microcavity, $P_{\text{coh}} = 0$. We consider the case of constant pumping:

$$P_{\text{incoh}}(\mathbf{r}) = \gamma_{\text{exR}}\rho_0 w(\mathbf{r}), \tag{19}$$

with the function $w(\mathbf{r})$ defining the spot profile

$$w(\mathbf{r}) = \exp\left[-\left(\frac{\mathbf{r}-\mathbf{r}_{\text{c}}}{\sigma_{\text{r}}}\right)^2\right]. \tag{20}$$

We place the pump spot centre at the origin, $\mathbf{r}_{\text{c}} = 0$. The value ρ_0 represents the maximum reservoir density in the equilibrium state. A value $\rho_0 = 0.5 \times 10^{12}\ cm^{-2}$ is utilized for numerical simulations of this section. The parameter $\sigma_{\text{r}} = 20\ \mu m$

sets the size of the pump spot. The values of $\gamma_{\rm cav}$, $\gamma_{\rm ex}$ and $\gamma_{\rm exR}$ are all determined by the corresponding lifetimes: $\tau_{\rm cav} = 1/\gamma_{\rm cav} = 3.8$ ps, $\tau_{\rm ex} = 1/\gamma_{\rm ex} = 1$ ns and $\tau_{\rm exR} = 1/\gamma_{\rm exR} = 10$ ps. The interexciton interaction constant $\alpha_{\rm c}$ is set to $6 \cdot 10^{-14}$ eV$\cdot$cm^2, the size of the grid cell $\Delta x = \Delta y = 0.5\ \mu m$. We consider the case of zero initial conditions

$$\psi(t=0) = \phi(t=0) = \rho_{\rm r}(t=0) = 0, \tag{21}$$

i.e. photon and exciton fluctuations play the role of the "seeds" for condensate nucleation.

In this case, the condensate formation develops a process of self-organization along with the gradual increase in condensate healing length. It is reasonable to assume that the dynamic memory in the Gross–Pitaevskii equation should contribute to this process. Since memory time is determined by the reservoir temperature, we expect significant influence of the latter on the dynamics of the system.

Numerical simulation results validate the latter assumption.

Figure 1 shows condensate density distributions for different temperatures and individual realizations of $\eta_{\rm cav}(\mathbf{r}, t)$ and $\eta_{\rm ex}(\mathbf{r}, t)$. All the cases correspond to $t = 130$ ps. By this time, all transients have finished, and the system reaches a quasi-equilibrium state.

As the data presented in Fig. 1 implies, the structure of this state is qualitatively different for various temperatures. At 5 and 20 K, the condensate occupies a broad

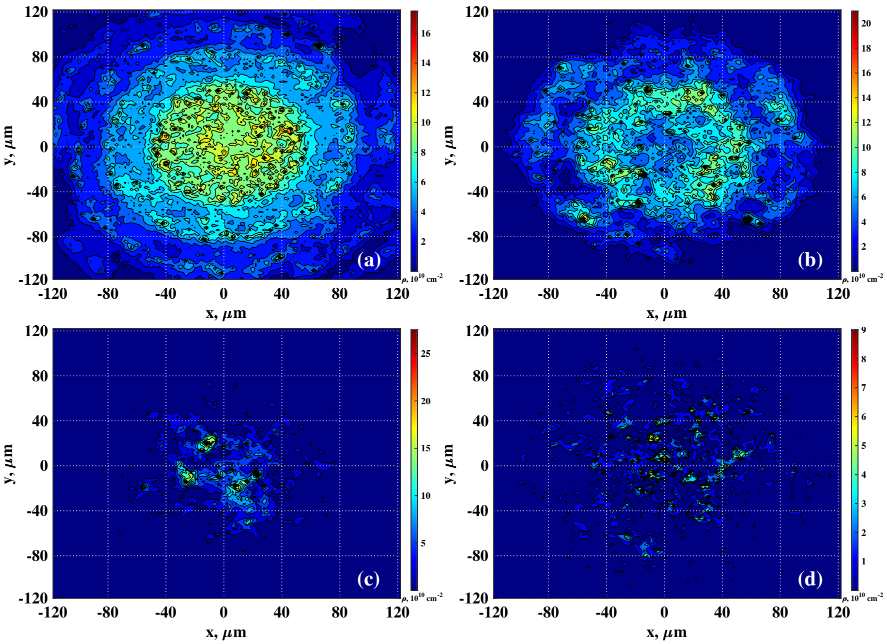

Fig. 1 Spatial distribution of condensate density at time $t = 130$ ps. Temperature values: **a** 5 K, **b** 20 K, **c** 35 K and **d** 50 K. All data presented correspond to a single realization of the fluctuation field

region, with the spatial density distribution roughly reproducing the intensity distribution in the incoherent pump beam. At 35 and 50 K, however, we observe the condensate individual irregular-shaped spots of condensate. This indicates that dynamic memory duration, which increases with decreasing temperature, plays a significant role in establishing the spatial correlations of the condensate.

The phenomenon of condensate fragmentation with increasing temperature was previously discussed in [20] for the case of spatially correlated fluctuations. Results of the present study with spatially uncorrelated fluctuations suggest that temporal correlations play a more important role in fragmentation of condensate.

Destruction of spatial correlations of the condensate with increasing temperature is more clearly demonstrated in Fig. 2, which depicts spatial condensate phase distributions for the same realizations as in Fig. 1. At $T = 5$ K, the constant phase lines arrange as concentric rings, somewhat distorted due to the presence of several singular points at the periphery, which correspond to vortex cores. Such a phase configuration indicates the presence of matter waves being emitted from the pump region with a regular wave front shape. At $T = 20$ K, the wave front undergoes significant spatial distortions due to the influence of spatial condensate fluctuations. With a further increase in temperature, the contribution of fluctuations increases, which leads eventually to the destruction of the ring phase configuration. At $T = 35$ K, traces of phase coherence are preserved only for individual condensate fragments, and at $T = 50$ K, they almost completely disappear.

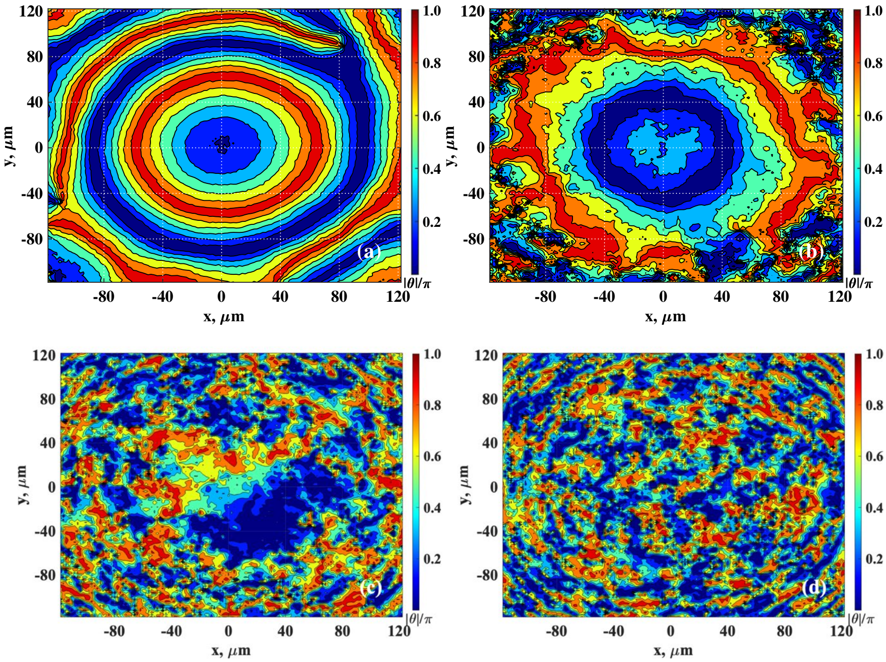

Fig. 2 Spatial distribution of the condensate phase absolute value at time $t = 130$ ps. The temperature values are as follows: **a** 5 K, **b** 20 K, **c** 35 K and **d** 50 K. All data presented correspond to a single realization of the fluctuation field

The behaviour of individual statistical realizations sheds light on the qualitative dependence of the condensate dynamics on the temperature, though statistical modelling is yet necessary.

4 Statistical Properties

4.1 Density Distribution

Foremost, we are interested in density distribution over the pumping spot, that's why we use the following definition for it:

$$\bar{\rho} = \frac{1}{\pi r_{\mathrm{c}}^2} \int d\mathbf{r} f(\mathbf{r}) |\psi(\mathbf{r})|^2 \tag{22}$$

where the function $f(\mathbf{r})$ picks out the regions of the pump spot with the highest density,

$$f(\mathbf{r}) = \begin{cases} 1, & |\mathbf{r} - \mathbf{r}_{\mathrm{c}}| \leq \sigma, \\ 0, & |\mathbf{r} - \mathbf{r}_{\mathrm{c}}| > \sigma. \end{cases} \tag{23}$$

As a statistical characteristic of density distribution, we use the scintillation index, which is defined as follows:

$$\mathrm{SI} = \frac{\langle \bar{\rho}^2 \rangle}{\langle \bar{\rho} \rangle^2} - 1. \tag{24}$$

The time dependence of $\bar{\rho}$ and scintillation index are presented in Fig. 3.

Foremost, we note that the low-temperature phase-ordered states (5 K and 20 K) demonstrate significantly higher densities and very weak spatial fluctuations. The sharp decrease in density that occurs with increasing temperature is accompanied by enhancement of fluctuations: We observe a pattern corresponding to the Berezinskii–Kosterlitz–Thouless(BKT) phase transition. At temperature $T = 35$ K, the condensate exists in the form of separate spots of high density on a turbulent background. This leads to high values of scintillation index, $\mathrm{SI} \simeq 2$. At $T = 50$ K, the contribution of such spots significantly decreases. As a consequence, the scintillation index approaches unity, which corresponds to the statistical saturation [23]. Also note that even after the condensate density stabilizes, it continues to exhibit slow oscillations. This may be due to the so-called relaxation oscillations [21, 24–26].

The transition of the condensate to a quasi-equilibrium regime with constant or slowly varying density corresponds to the onset of a balance between pumping from the reservoir and decay. The presence of such a balance may indicate the emergence of a state with PT (parity-time) symmetry [27]. In this case, the energy spectrum becomes real despite the non-Hermiticity of exciton–polaritons. The appearance of PT symmetry in a system with memory has been considered earlier in [28].

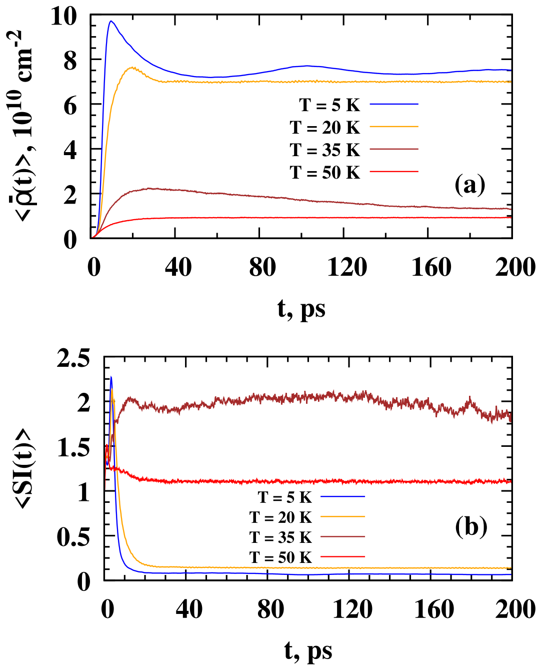

Fig. 3 Time dependencies of ensemble-averaged density $\bar{\rho}$ (panel **a**) and the scintillation index (panel **b**) for different temperature values

4.2 Quantifying Coherence

To trace how the coherent properties of the condensate evolve, we evaluate the fixed time first-order coherence function.

$$g^{(1)}(\Delta\mathbf{r}, t) = \frac{|\langle \psi^*(\mathbf{r} + \Delta\mathbf{r}/2, t)\psi(\mathbf{r} - \Delta\mathbf{r}/2, t)\rangle|}{\left\langle \sqrt{\rho_c(\mathbf{r} + \Delta\mathbf{r}/2, t)\rho_c(\mathbf{r} - \Delta\mathbf{r}/2, t)} \right\rangle}, \tag{25}$$

with $\rho_c(\mathbf{r}, t) = |\psi(\mathbf{r}, t)|^2$ being the condensate density. We use fixed $\mathbf{r} = \mathbf{0}$ and average over the angular part of $\Delta\mathbf{r}$ to observe radial decrease in coherence. The results are demonstrated in Fig. 4 for various reservoir densities (i.e. pumping intensities) and fixed temperature $T = 20$ K.

Low-density system demonstrates negligible coherence (a). In panel (b), one may estimate coherence radii at various times, thus tracing coherence build-up. Plots (c) and (d) illustrate similar evolution, which implies saturation of coherence radius, which approaches the boundary of the pumping area. In this regime, we observe phase coherence throughout the pumping spot.

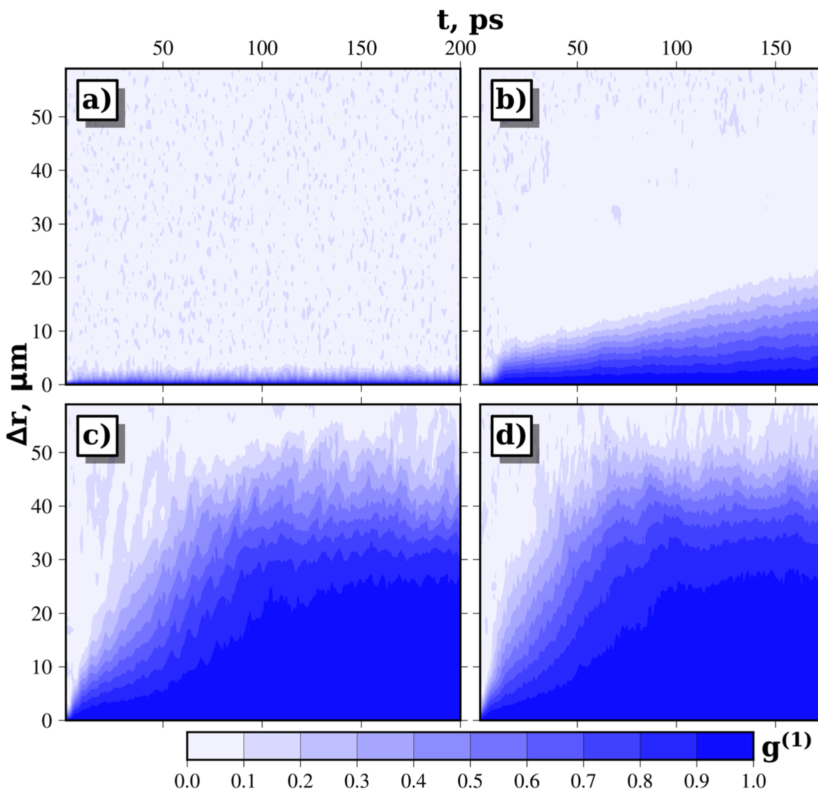

Fig. 4 Colour maps show the fixed time first-order correlation function (4) evolution for varying intensity of incoherent pumping, quantified by the maximum reservoir density ρ_0. **a** $\rho_0 = 0.2 \times 10^{11}$ cm^{-2}, **b** $\rho_0 = 0.1 \times 10^{12}$ cm^{-2}, **c** $\rho_0 = 0.5 \times 10^{11}$ cm^{-2} and **d** $\rho_0 = 2 \times 10^{12}$ cm^{-2}

4.3 Spectral Properties

In order to study condensate decoherence with increasing temperature, one may trace changes in the spectrum during condensate formation. We studied the optical radiation of the condensate for this purpose.

To simplify the analysis, we eliminate spatial degrees of freedom by means of a weighted integration, with the weight function being given by the pumping profile:

$$\Psi_{\text{eff}}(t) = \frac{\int d\mathbf{r}w(\mathbf{r})\psi(\mathbf{r},t)}{\int d\mathbf{r}w(\mathbf{r})}. \tag{26}$$

To obtain the spectrum of the signal, we use the Gabor transform, which is a kind of the Fourier window transform with the Gaussian window:

$$g_W(\nu,t) = \int_{-\infty}^{\infty} \mathrm{d}t' \Psi_{\text{eff}}(t')\chi_{\text{W}}(\nu,t'-t),$$

where $\chi_W(\nu, t) = R_W(t) \exp(2\pi i \nu t)$ and

$$R_W(t) = \frac{1}{\sqrt{W\sqrt{2\pi}}} \exp\left(-\frac{t^2}{4W^2}\right). \tag{27}$$

The window is centred at $t = t'$, and W sets its size. By moving the centre of the window along the time axis, one may trace the time dependence of the frequency spectrum of $\Psi_{\text{eff}}(t)$.

Figure 5 shows the spectral density of the signal averaged over 100 realizations. One may observe that at temperatures 5 K and 20 K, the condensate is concentrated in low-energy states within a narrow spectral band. The mean frequency of this band corresponds to the equilibrium chemical potential. Its increase with increasing temperature is associated with enhancement of the condensate inhomogeneity and, as a consequence, higher contribution of kinetic energy.

At 35 K, the condensate spectrum is still given by a fairly narrow band, but the shape and intensity of this band changes with time. Comparing the evolution of the spectrum with the data presented in Fig. 3a, one may conclude that the decay is not completely compensated by pumping. This may be due to the metastability of condensate spots arising at 35 K.

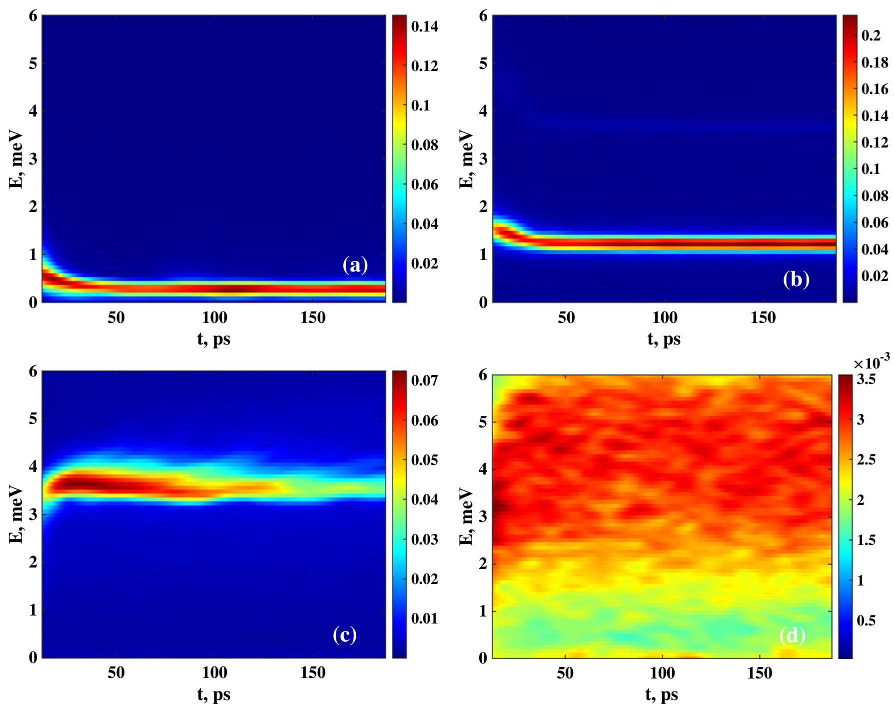

Fig. 5 Optical radiation spectrum of the condensate obtained using the Gabor transform. Temperature values: **a** 5 K, **b** 20 K, **c** 35 K and **d** 50 K

5 Conclusion

Due to their low effective mass, exciton–polaritons are known as possible candidates for creation of room temperature condensates, and study of temperature effects is very meaningful in this context. In the present paper, we have presented a non-Markovian stochastic Gross–Pitaevskii model for the exciton–polariton Bose–Einstein condensation. We used it to study the influence of the temperature on the condensate formation process in the absence of coherent pumping. The results obtained reveal the complex structure of the transition from the coherent to the disordered phase. In particular, one may note the appearance of dense condensate spots on the turbulent background, detected at 35 K. Due to the presence of these spots, the spectrum of the optical signal emitted by the condensate is a narrow-band one.

Further work in this field will be devoted to the improvement of the model used to describe the condensate and the reservoir. Another promising way is study of modulational instability of the condensate that could provide theoretical prediction of the fragmentation crossover observed in the present paper. Also, it is reasonable to study the impact of the coherent photonic pumping to test on stabilizing condensate coherence.

Acknowledgements The authors are grateful to anonymous referees for valuable comments and to M. Uleysky for the assistance in the preparation of figures. The work of A. Alliluev and D. Makarov is supported by the Laboratory of Nonlinear Hydrophysics and Natural Hazards of the V.I.Il'ichev Pacific Oceanological Institute of the Far Eastern Branch of the Russian Academy of Sciences, within the project of the Ministry of Science and Higher Education of the Russian Federation, agreement number 075-15-2022-1127. N. Asriyan is supported by the foundation for the advancement of theoretical physics and mathematics "Basis". Yu. Lozovik's work is supported by the Russian Science Foundation (RSF) in the scope of the project 23-12-00115.

Author Contributions YE supervised this work. DV, NA and AA contributed to the theoretical part of the paper. AD and DV performed the numerical simulations. DV and NA contributed to writiing of the text. AD prepared illustrations for the paper.

Declarations

Conflict of Interest The authors declare no competing interests.

References

1. H.-P. Breuer, F. Petruccione, *The Theory of Open Quantum Systems* (Oxford University Press, Oxford, 2007)
2. A.R. Kolovsky, D.L. Shepelyansky, Ann. Phys. Berlin **531**, 1900231 (2019)
3. H.T.C. Stoof, M.J. Bijlsma, J. Low. Temp. Phys. **124**, 431 (2001)
4. S.P. Cockburn, N.P. Proukakis, Laser Phys. **19**, 558 (2009)
5. I. De Vega, D. Alonso, Rev. Mod. Phys. **89**, 015001 (2017)
6. S. Nakajima, Progr. Theor. Phys. **20**, 948 (1958)
7. R. Zwanzig, J. Chem. Phys. **83**, 1338 (1960)
8. H.-P. Breuer, Phys. Rev. A **70**, 012106 (2004)
9. H.-P. Breuer, E.-M. Laine, J. Piilo, B. Vacchini, Rev. Mod. Phys. **88**, 021002 (2016)
10. L. Diósi, W.T. Strunz, Phys. Lett. A **235**, 569 (1997)

11. A.A. Elistratov, Yu.E. Lozovik, Phys. Rev. B **93**, 014525 (2018)
12. Y. Xue, X. Ma, A. Kavokin et al., Phys. Rev. Res. **3**, 013099 (2021)
13. S. Kim et al., Phys. Rev. X **6**, 011026 (2016)
14. J. Kasprzak et al., Nature **443**, 409 (2006)
15. V.B. Timofeev, Semiconductors **46**, 843 (2012)
16. F. Manni et al., PRL **107**, 106401 (2011)
17. F. Baboux et al., Optica **5**(10), 1163–1170 (2018)
18. M. Pieczarka et al., Nat. Commun. **11**, 429 (2020)
19. S.S. Gavrilov, Phys. Uspekhi **63**(2), 123 (2020)
20. A.D. Alliluev, D.V. Makarov, N.A. Asriyan, A.A. Elistratov, Yu.E. Lozovik, Phys. Lett. A **453**, 128492 (2022)
21. D.V. Makarov, A.A. Elistratov, Yu.E. Lozovik, Phys. Lett. A **384**, 126942 (2020)
22. X. Li, Phys. Lett. A **387**, 127036 (2021)
23. R. Dashen, J. Math. Phys. **20**, 894 (1979)
24. M. De Giorgi et al., Phys. Rev. Lett. **112**, 113602 (2014)
25. A. Opala, M. Pieczarka, M. Matuszewski, Phys. Rev. B **98**, 195312 (2018)
26. C. Tian et al., Nano Lett. **22**, 3026 (2022)
27. IYu. Chestnov et al., Sci. Rep. **22**, 3026 (2022)
28. Z.A. Cochran, A. Saxena, Y.N. Joglekar, Phys. Rev. Res. **3**, 013135 (2021)